Supporting Information

A porous nickel cyclotetraphosphate nanosheet as a new acid-stable electrocatalyst for efficient hydrogen evolution

Xiong Liu,‡ Bo Wen,‡ Ruiting Guo,‡ Jiashen Meng, Ziang Liu, Wei Yang, Chaojiang Niu, Qi Li,* and Liqiang Mai*

State Key Laboratory of Advanced Technology for Materials Synthesis and Processing, Wuhan University of Technology, Wuhan 430070, China

Experimental section

Synthesis of the porous $Ni_2P_4O_{12}$ nanosheets grown on carbon cloth ($Ni_2P_4O_{12}$/CC).

The synthesized method refers to the previous reports with some modifications.[1] Firstly, 3 mmol of nickel (Ⅱ) nitrate hexahydrate ($Ni(NO_3)_2 \cdot 6H_2O$), 2 mmol of ammonium fluoride (NH_4F), 5 mmol urea ($CO(NH_2)_2$) were dissolved into 35 mL of deionized water. Then the uniform solution and a piece of the pretreated carbon cloth (2 cm × 4 cm) were enclosed into a 50 mL Teflon-lined stainless steel autoclave and heated at 120 °C for 5 h. After cooling, the nickel hydroxide hydrate nanosheets grown on carbon cloth (denoted as $Ni(OH)_2 \cdot 0.75H_2O$/CC) were washed, heated to 350 °C and maintained for 2 h in air to obtain the nickel oxide nanosheets grown on carbon cloth (denoted as NiO/CC). For the phosphorylation treatment, a piece of NiO/CC and 0.6 g of $NaH_2PO_2 \cdot H_2O$ were placed at two different areas in a tubular furnace, then heated to 320 °C and maintained in Ar for 2 h. After cooling down to room temperature, the sample was washed, dried and finally the $Ni_2P_4O_{12}$/CC was obtained. Noted that the PH_3 gas is very dangerous, toxic and flammable. Therefore, after cooling down to room temperature, the gas treatment was performed with the $CuSO_4$ solution. The PH_3 gas exposed to air may burn automatically if the temperature is higher than 50 °C.

Structural Characterization

X-ray diffraction (XRD) was conducted using a Bruker D8 Advance X-ray diffractometer with a nonmonochromated Cu Kα X-ray source. Scanning electron microscopy (SEM) images were collected with a JEOL-7100F microscope at an acceleration voltage of 25 kV. Transmission electron microscopy (TEM), high-resolution transmission electron microscopy (HRTEM), high-angle annular dark-field scanning transmission electron microscopy (HAADF-STEM), energy-dispersive (EDS) maps and the selected area electron diffraction (SAED) were recorded by using a JEM-2100F STEM/EDS microscope. Brunauer-Emmett-Teller (BET) surface areas

were measured using a Tristar II 3020 instrument by adsorption of nitrogen at 77 K. X-ray photoelectron spectra (XPS) was performed using a VG Multi Lab 2000 instrument. FTIR spectra were obtained using Nicolet6700 spectroscopy. Atomic Force Microscope (AFM) measurements were mearsurd by SmartSPM™ 1000 (AIST-NT) with the aluminum coating n-type silicon probe (μmasch, HQ: NSC14/AIB5, 125 μm, 160 kHz, 5 N/M).

Electrochemical measurement

The HER activity of samples was measured using a three-electrode system on an electrochemical workstation (CHI760D) at room temperature. A saturated calomel electrode (SCE, saturated KCl) was used as a reference electrode, a graphite rod was used as a counter electrode and the catalysts supported on carbon cloth were directly used as a working electrode to test the electrocatalytic activity in 0.5 M H_2SO_4. LSV measurements were carried out at a slow sweep rate of 5 mV s^{-1} to eliminate the capacitive current during the electrocatalytic reaction as much as possible. The data were corrected with the iR compensation according to the equation ($E_{corr} = E_{mea} - iR_s$) to remove the influence of Ohmic resistance. E_{corr} is the iR compensated potential, E_{mea} is the measured potential and R_s is obtained via the iR compensation on the test system. Electrochemical impedance spectroscopy (EIS) was tested in a frequency ranging from 0.1 Hz to 100,000 Hz. The long-term durability testing was carried out at -10 mA cm^{-2}. To get the dependence between the current density and the applied potential, the steady-state current density as a function of voltage was measured with a dwell time of 5 min.

To obtain the electrochemical double layer capacitance and estimate the effective active surface area of all samples, CV measurements were carried out at non-faradaic potentials. In detail, CV measurements were performed at various scan rates (2, 4, 6, 8 and 10 mV s^{-1}) in -0.1 ~ -0.2 V *vs.* SCE. By plotting the difference of current density (ΔJ) between the anodic and cathodic sweeps ($\Delta J = J_{anodic} - J_{cathodic}$) at 0.13 V *vs.* RHE against the scan rate, a linear trend was observed. The slope of the fitting curve is equal to twice the geometric double layer capacitance (C_{dl}), which is proportional to the electrochemical active surface area of catalysts. The Faradaic efficiency is calculated by applying a constant potential (-0.6 V *vs.* SCE) on the electrode and the volume of the evolved hydrogen gas was collected by the water drainage method. The detailed method refers to the previous reports.[2,3]

The commercial Pt/C (20 wt.%) powder was tested as a control sample. The Pt/C catalyst supported on carbon cloth was prepared via dispersing 8 mg of Pt/C and 2 mg of Vulcan XC-72R in the mix of 700 μL isopropyl alcohol, 250 μL deionized water and

50 μL Nafion solution (5 wt.%) with sonication for 0.5 h to form a homogeneous ink, then the 125 μL of ink was coated on carbon cloth within 1 cm^2 area. All the potentials were referenced to a reversible hydrogen electrode (RHE) based on the equation: $E(RHE) = E(SCE) + 0.2415\ V + 0.0592 \times pH$.

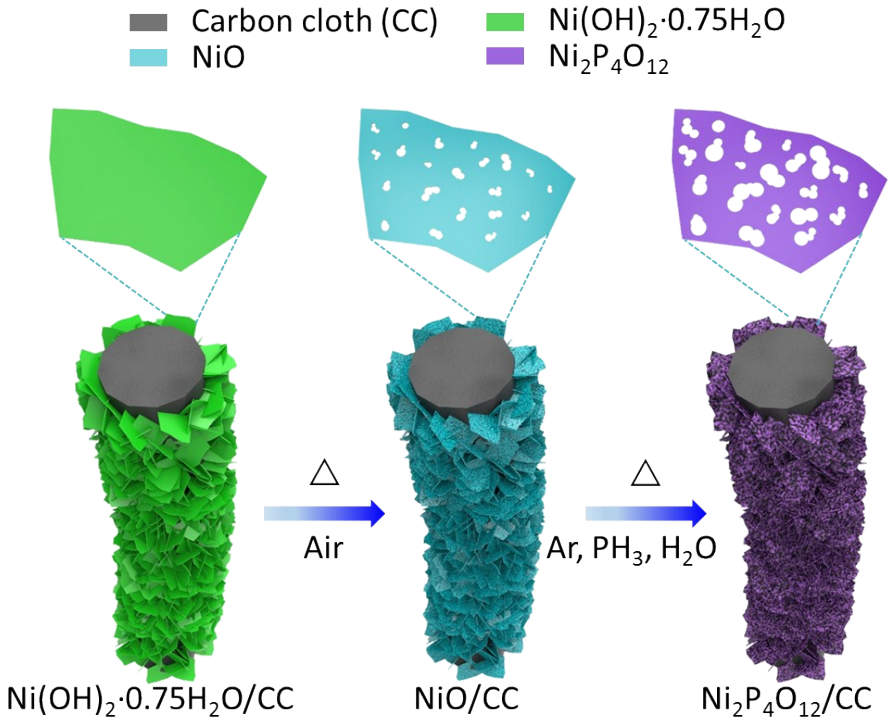

Fig. S1 Schematic illustration of the synthesis procedure of $Ni_2P_4O_{12}$/CC.

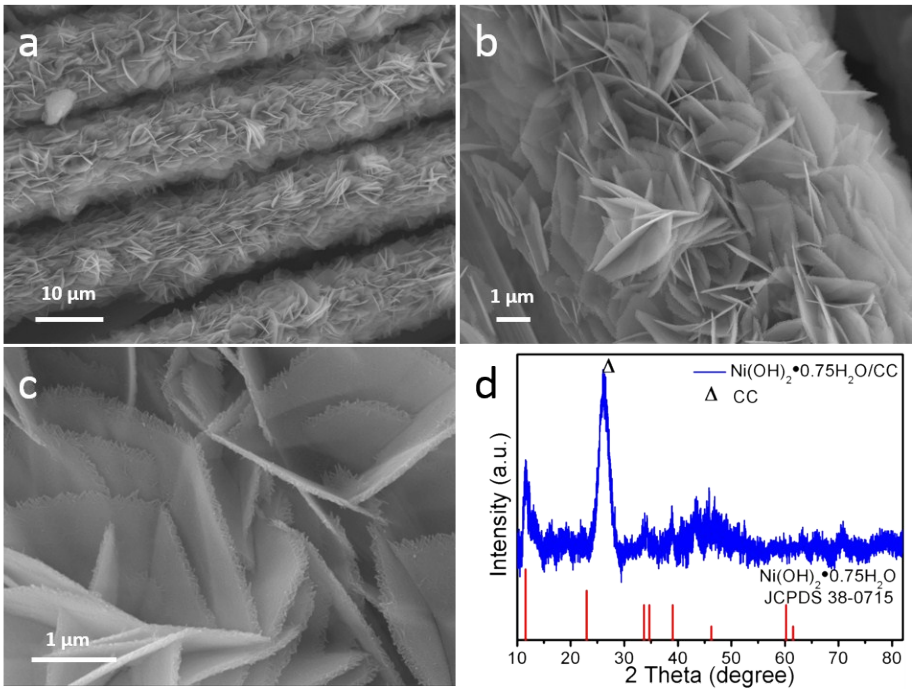

Fig. S2 (a-c) SEM images and (d) XRD pattern of $Ni(OH)_2 \cdot 0.75H_2O$/CC.

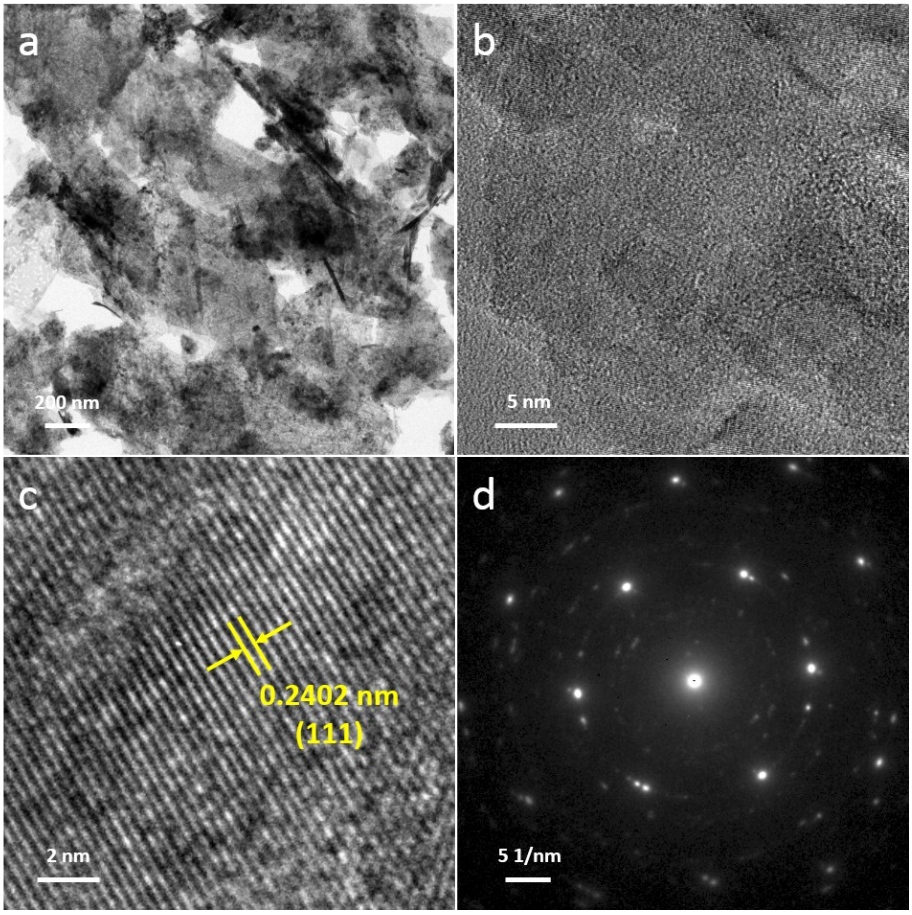

Fig. S3 (a,b) TEM images, (c) HRTEM image and (d) SAED pattern of the NiO nanosheets obtained from NiO/CC.

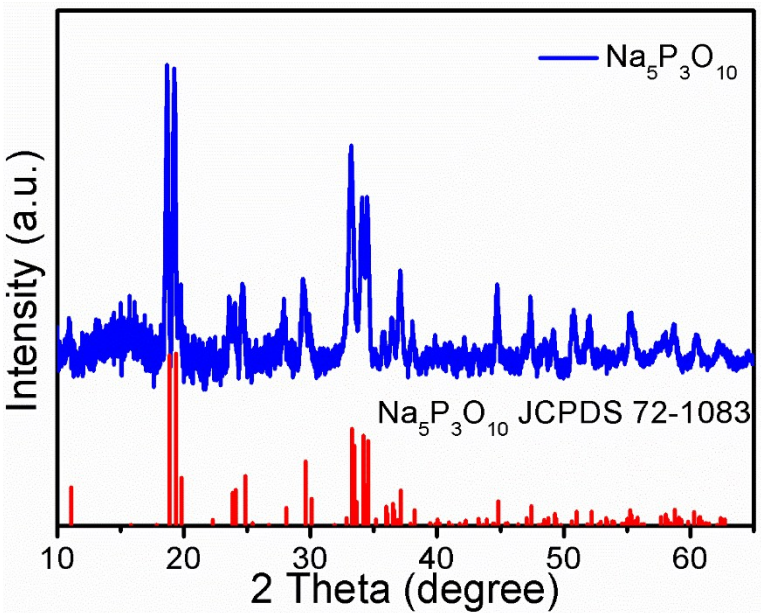

Fig. S4 XRD pattern for the residuals of $NaH_2PO_2 \cdot H_2O$ after calcination in Ar.

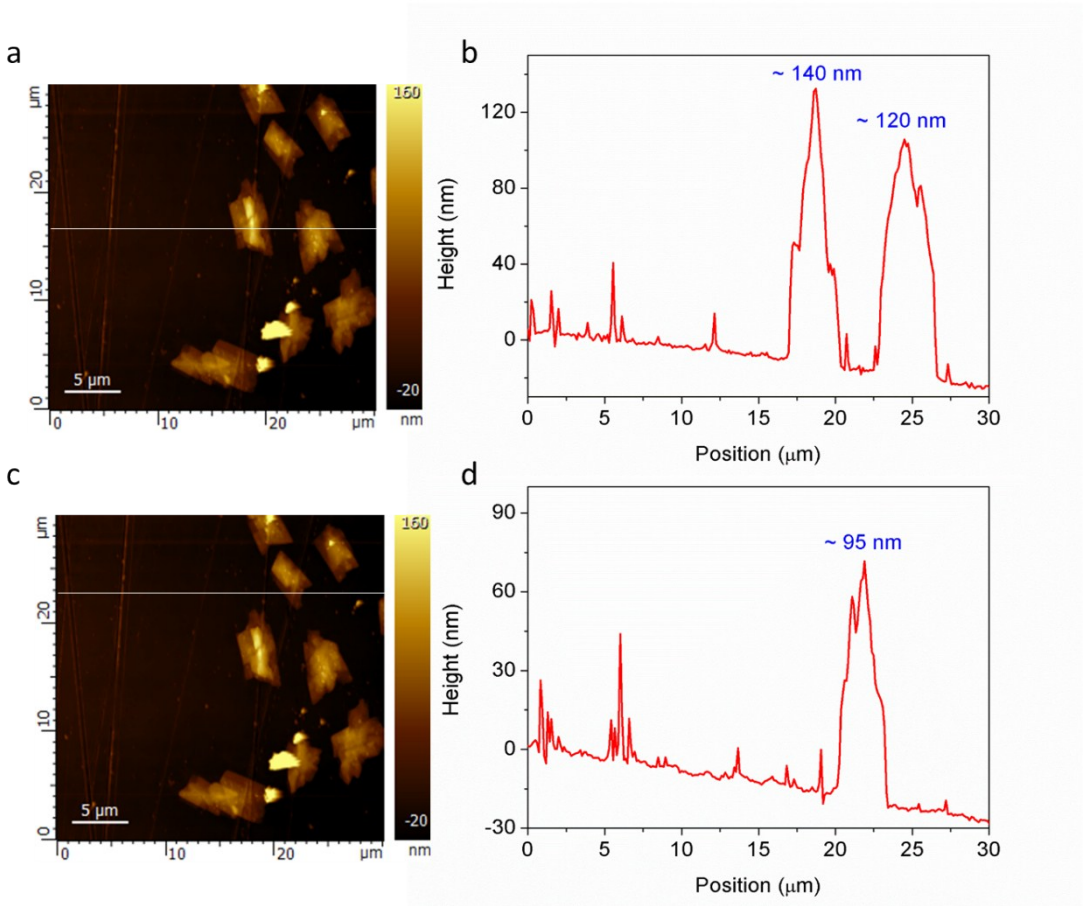

Fig. S5 (a,c) AFM images of the obtained $Ni_2P_4O_{12}$ nanosheets. (b,d) The corresponding height profiles along the white line in (a) and (c), respectively.

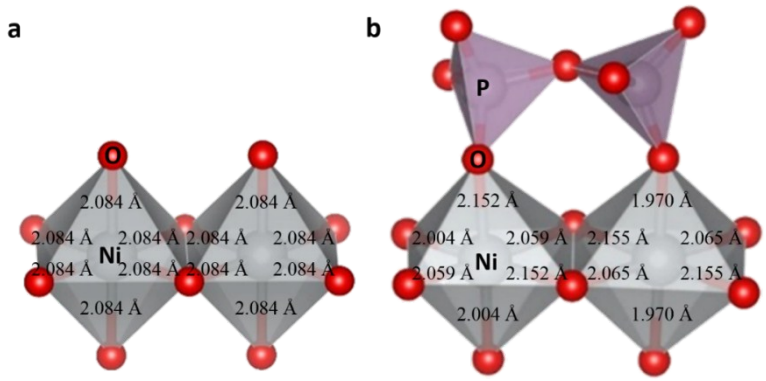

Fig. S6 Bond lengths of (a) NiO and (b) $Ni_2P_4O_{12}$ crystals, respectively.

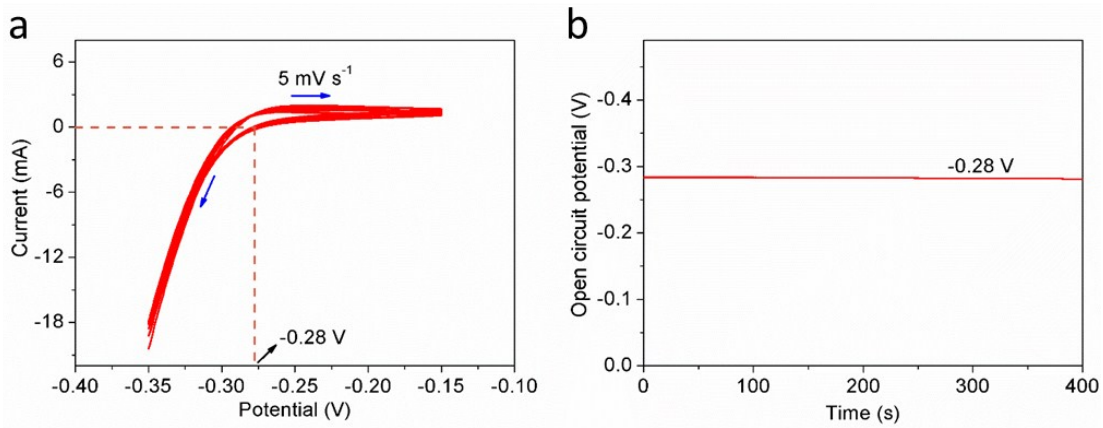

Fig. S7 Calibration of SCE. (a) CV curve of hydrogen oxidation and evolution in 0.5 M H_2SO_4. (b) Open circuit potential of the electrochemical cell.

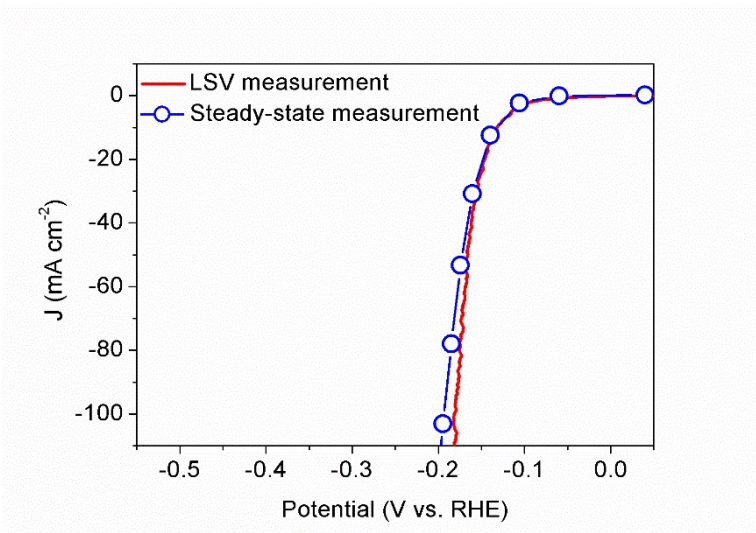

Fig. S8 LSV measurement and steady-state measurement of $Ni_2P_4O_{12}$/CC in 0.5 M H_2SO_4 for HER.

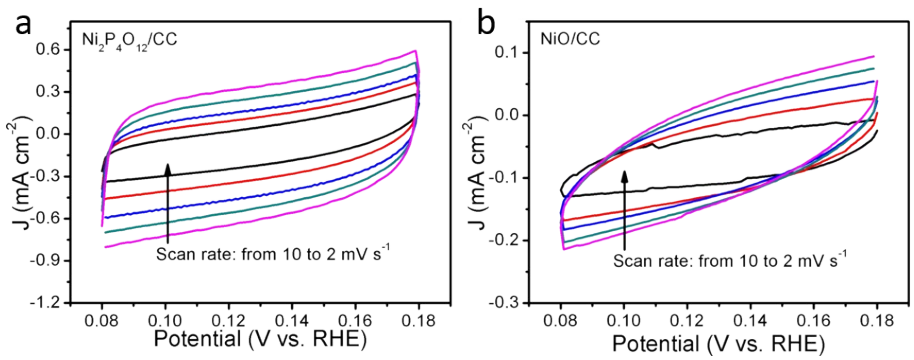

Fig. S9 CV curves of a) $Ni_2P_4O_{12}$/CC and b) NiO/CC at various scan rates. The current densities obtained at 0.13 V *vs.* RHE are used to calculate the C_{dl} values.

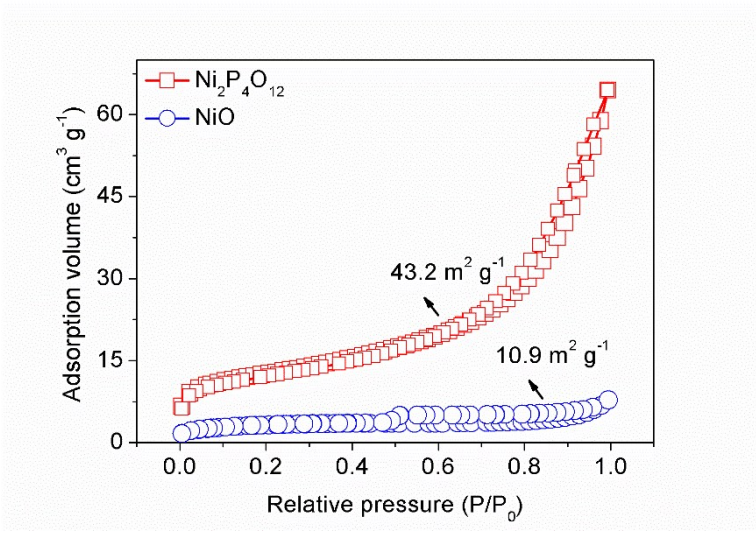

Fig. S10 N_2 adsorption/desorption isotherms of the $Ni_2P_4O_{12}$ and NiO nanosheets.

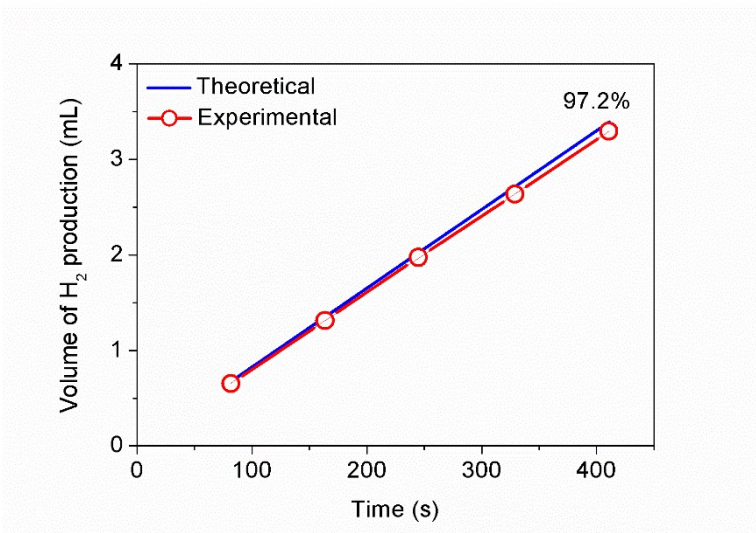

Fig. S11 Experimental hydrogen gas evolution during electrolysis and theoretical amount of hydrogen gas.

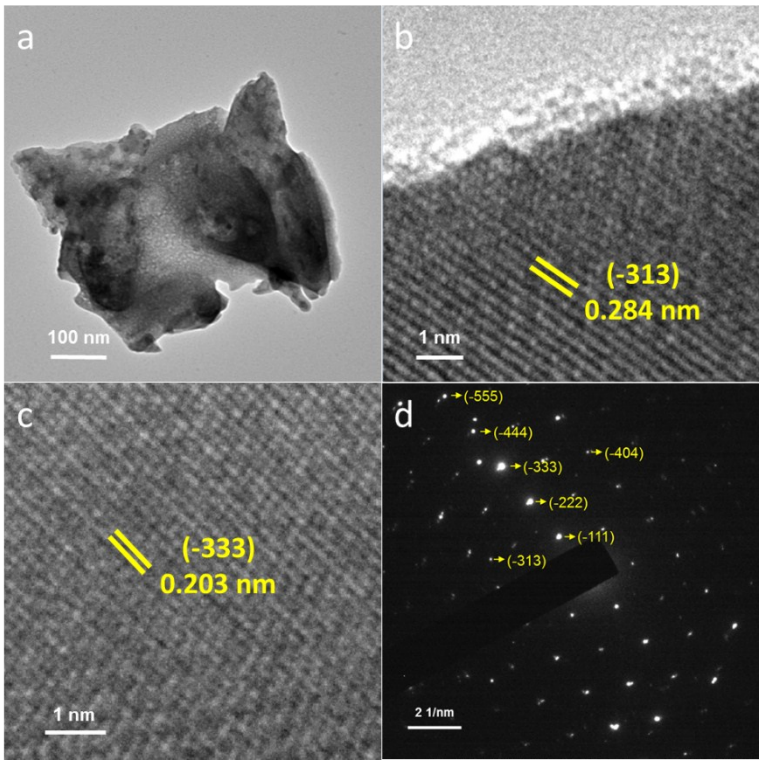

Fig. S12 (a) TEM, (b,c) HRTEM images and (d) SAED pattern of $Ni_2P_4O_{12}$/CC after long-term durability testing.

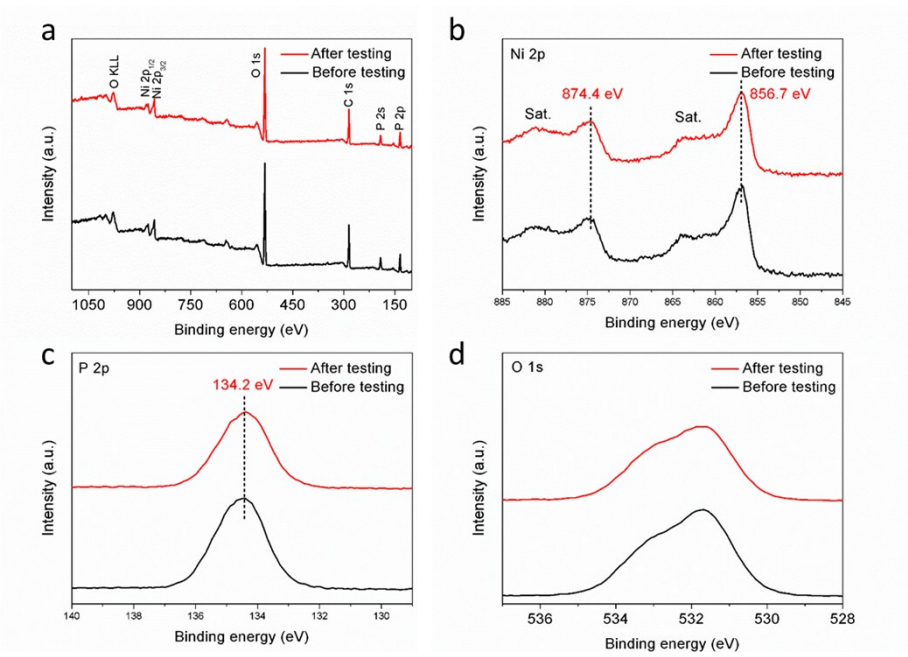

Fig. S13 XPS spectra of $Ni_2P_4O_{12}$/CC before and after long-term durability testing: (a) survey scan, (b) Ni 2p, (c) P 2p and (d) O 1s.

Table S1. Summary of the surface species on the reported transition metal phosphides based catalysts before the catalytic measurements. Note that the CC, NC, BCN, NSs, CNT, TM and NWs represent the carbon cloth, N-doped carbon, B/N-doped carbon, nanosheets, carbon nanotubes, nanotubes, titanium mesh and nanowires, respectively.

Catalysts	Surface species	References
FeP, $Fe_{0.5}Co_{0.5}P$[4]	Phosphate species (PO_4^{3-})	*Energy Environ. Sci.*, 2015, **8**, 3022-3029
Mo-W-P NSs/CC[5]	Oxidized phosphorus species	*Energy Environ. Sci.*, 2016, **9**, 1468-1475
MoP NPs[6]	Oxidized P species	*Adv. Mater.*, 2014, **26**, 5702-5707
WP_2 NWs/CC[7]	Oxidized P species	*Nanoscale*, 2016, **8**, 19779-19786
CoP nanoneedles/CC[8]	Co_3O_4, $Co(PO_x)_y$	*ChemSusChem*, 2016, **9**, 472-477
Ni_2P[9]	PO_4^{3-} species	*Angew. Chem. In. Ed.*, 2016, **128**, 4098-4102
Ni_2P[10]	$H_2PO_3^-$	*J. Phys. Chem. C*, 2015, **119**, 2557-2565
$Zn_{0.08}Co_{0.92}P$/TM[11]	Oxidized phosphate species	*Adv. Energy Mater.*, 2017, **7**, 1700020
M−Co_2P/NCNTs (M = Fe, Ni, Cu)[12]	Oxidized P species	*ACS Appl. Mater. Interfaces*, 2016, **8**, 13890-13901
CoP/MoS_2-CNTs[13]	Oxidized P species	*Catal. Sci. Technol.*, 2016, **6**, 1611-1615
CoS|P/CNT[14]	Phosphate-like P	*Nat. Commun.*, 2016, **7**, 10771
CoP@BCN nanotubes[15]	P-O oxidized species of phosphide	*Adv. Energy Mater.*, 2017, **7**, 1601671
Ni/NiP[16]	Oxidized P species	*Adv. Funct. Mater.*, 2016, **26**, 3314-3323
PANI/CoP NWs[17]	$CoPO_x$	*J. Am. Chem. Soc.*, 2018, **140**, 5118-5126
$Ni_{0.51}Co_{0.49}P$ film[18]	Oxidized P species	*Adv. Funct. Mater.*, 2016, **26**, 7644-7651
NiCoP/CC[19]	PO_4^{3-} or P_2O_5	*ACS Catal.*, 2017, **7**, 4131-4137

Table S2. Comparison of the acidic HER performance in this work with the non-precious metal-based electrocatalysts reported previously. Note that the CC, NSs, NPs, NTs, NAs and NWs represent the carbon cloth, nanosheets, nanoparticles, nanotubes, nanorod arrays and nanowires, respectively.

Catalysts	η_{10} (mV)	Tafel slope (mV dec^{-1})	References
$Ni_2P_4O_{12}$/CC	131.8	47.8	This work
Ni-P NSs/CC[20]	98	58.8	*Adv. Funct. Mater.*, 2016, **26**, 4067-4077
NiP_2 NSs/CC[21]	75	51	*Nanoscale*, 2014, **6**, 13440-13445
Ni_2P NPs[22]	<130	~46	*J. Am. Chem. Soc.*, 2013, **135**, 9267-9270
Ni_3N NSs[23]	59	59.8	*J. Mater. Chem. A*, 2016, **4**, 17363-17369
Ni-W NPs[24]	205	122	*Mater. Lett.*, 2018, **213**, 15-18
MoP_2 NPs /Mo plate[25]	143	57	*Nanoscale*, 2016, **8**, 8500-8504
$CoSe_2$ NPs/CC[26]	137	42.1	*J. Am. Chem. Soc.*, 2014, **136**, 4897-4900
CoP NTs[27]	129	60	*J. Mater. Chem. A*, 2014, **2**, 14812-14816
FeP NAs/CC[28]	58	45	*ACS Catal.*, 2014, **4**, 4065-4069
WP_2 NWs/CC[7]	109	56	*Nanoscale*, 2016, **8**, 19779-19786

References

1 Q. Liu, C. Y. Chen, J. J. Zheng, L. Wang, Z. B. Yang, W. Y. Yang, *J. Mater. Chem. A*, 2017, **5**, 1421-1427.

2 Z. L. Wang, X. F. Hao, Z. Jiang, X. P. Sun, D. Xu, J. Wang, H. X. Zhong, F. L. Meng, X. B. Zhang, *J. Am. Chem. Soc.*, 2015, **137**, 15070-15073.

3 L. L. Feng, G. T. Yu, Y. Y. Wu, G. D. Li, H. Li, Y. Y. Sun, T. Asefa, W. Chen, X. X. Zou. *J. Am. Chem. Soc.*, 2015, **137**, 14023-14026.

4 J. Kibsgaard, C. Tsai, K. Chan, J. D. Benck, J. K. Nørskov, F. Abild-Pedersen, T. F. Jaramillo, *Energy Environ. Sci.*, 2015, **8**, 3022-3029.

5 X. D. Wang, Y. F. Xu, H. S. Rao, W. J. Xu, H. Y. Chen, W. X. Zhang, D. B. Kuang, C. Y. Su, *Energy Environ. Sci.*, 2016, **9**, 1468-1475.

6 Z. C. Xing, Q. Liu, A. M. Asiri, X. P. Sun, *Adv. Mater.*, 2014, **26**, 5702-5707.

7 M. Y. Pi, T. L. Wu, D. K. Zhang, S. J. Chen, S. X. Wang, *Nanoscale*, 2016, **8**, 19779-19786.

8 P. Wang, F. Song, R. Amal, Y. H. Ng, X. L. Hu, *ChemSusChem*, 2016, **9**, 472-477.

9 S. Tian, X. Li, A. J. Wang, R. Prins, Y. Y. Chen, Y. K. Hu, *Angew. Chem. Int. Ed.*,

2016, **55**, 4030-4034.

10 R. G. Li, Q. X. Guan, R. C. Wei, S. Q. Yang, Z. Shu, Y. Dong, J. Chen, W. Li, *J. Phys. Chem. C*, 2015, **119**, 2557-2565.

11 T. T. Liu, D. N. Liu, F. L. Qu, D. X. Wang, L. Zhang, R. X. Ge, S. Hao, Y. J. Ma, G. Du, A. M. Asiri, L. Chen, X. P. Sun, *Adv. Energy Mater.*, 2017, **7**, 1700020.

12 Y. Pan, Y. Lin, Y. Q. Liu, C. G. Liu, *Catal. Sci. Technol.*, 2016, **6**, 1611-1615.

13 Y. Pan, Y. Q. Liu, Y. Lin, C. G. Liu, *ACS Appl. Mater. Interfaces*, 2016, **8**, 13890-13901.

14 W. Liu, E. Y. Hu, H. Jiang, Y. J. Xiang, Z. Weng, M. Li, Q. Fan, X. Q. Yu, E. I. Altman, H. L. Wang, *Nat. Commun.*, 2016, **7**, 10771-10779.

15 H. Tabassum, W. H. Guo, W. Meng, A. Mahmood, R. Zhao, Q. F. Wang, R. Q. Zou, *Adv. Energy Mater.*, 2017, **7**, 1601671.

16 G.-F. Chen, T. Y. Ma, Z.-Q. Liu, N. Li, Y.-Z. Su, K. Davey, S.-Z. Qiao, *Adv. Funct. Mater.*, 2016, **26**, 3314-3323.

17 J. X. Feng, S. Y. Tong, Y. X. Tong, G. R. Li, *J. Am. Chem. Soc.*, 2018, **140**, 5118-5126.

18 J. Yu, Q. Q. Li, Y. Li, C.-Y. Xu, L. Zhen, V. P. Dravid, J. S. Wu, *Adv. Funct. Mater.*, 2016, **26**, 7644-7651.

19 C. Du, L. Yang, F. L. Yang, G. Z. Cheng, W. Luo, *ACS Catal.*, 2017, **7**, 4131-4137.

20 X. G. Wang, W. Li, D. H. Xiong, D. Y. Petrovykh, L. F. Liu, *Adv. Funct. Mater.*, 2016, **26**, 4067-4077.

21 P. Jiang, Q. Liu, X. P. Sun, *Nanoscale*, 2014, **6**, 13440-13445.

22 E. J. Popczun, J. R. McKone, C. G. Read, A. J. Biacchi, A. M. Wiltrout, N. S. Lewis and R. E. Schaak, *J. Am. Chem. Soc.*, 2013, **135**, 9267-9270.

23 D. Q. Gao, J. Y. Zhang, T. T. Wang, W. Xiao, K. Tao, D. S. Xue, J. Ding, *J. Mater. Chem. A*, 2016, **4**, 17363-17369.

24 Y. B. Mollamahale, N. Jafari, D. Hosseini, *Mater. Lett.*, 2018, **213**, 15-18

25 Z. H. Pu, I. Saana Amiinu, M. Wang, Y. S. Yang, S. C. Mu, *Nanoscale*, 2016, **8**, 8500-8504.

26 D. S. Kong, H. T. Wang, Z. Y. Lu, Y. Cui, *J. Am. Chem. Soc.*, 2014, **136**, 4897-4900.

27 H. F. Du, Q. Liu, N. Y. Cheng, A. M. Asiri, X. P. Sun, C. M. Li, *J. Mater. Chem. A*, 2014, **2**, 14812-14816.

28 Y. H. Liang, Q. Liu, A. M. Asiri, X. P. Sun, Y. L. Luo, *ACS Catal.*, 2014, **4**, 4065-4069.